European Journal of Neuroscience, Vol. 20, pp. 1788–1802, 2004

Synaptic release of dopamine in the subthalamic nucleus

Stephanie J. Cragg,[1] Jérôme Baufreton,[2,4] Yi Xue,[2] J. Paul Bolam[3] and Mark D. Bevan[2,3,4]
[1]Department of Pharmacology, University of Oxford, Oxford OX1 3QT, UK
[2]University of Tennessee, Department of Anatomy & Neurobiology, Memphis, TN 38163, USA
[3]MRC Anatomical Neuropharmacology Unit, Oxford OX1 3TH, UK
[4]Northwestern University, Department of Physiology, Feinberg School of Medicine, 303 East Chicago Avenue, Chicago, IL 60611-3008, USA

Keywords: basal ganglia, dopamine transporter, dopaminergic, rat, synapse

Abstract

The direct modulation of subthalamic nucleus (STN) neurons by dopamine (DA) neurons of the substantia nigra (SN) is controversial owing to the thick caliber and low density of DA axons in the STN. The abnormal activity of the STN in Parkinson's disease (PD), which is central to the appearance of symptoms, is therefore thought to result from the loss of DA in the striatum. We carried out three experiments in rats to explore the function of DA in the STN: (i) light and electron microscopic analysis of tyrosine hydroxylase (TH)-, dopamine β-hydroxylase (DβH)- and DA-immunoreactive structures to determine whether DA axons form synapses; (ii) fast-scan cyclic voltammetry (FCV) to determine whether DA axons release DA; and (iii) patch clamp recording to determine whether DA, at a concentration similar to that detected by FCV, can modulate activity and synaptic transmission/integration. TH- and DA-immunoreactive axons mostly formed symmetric synapses. Because DβH-immunoreactive axons were rare and formed asymmetric synapses, they comprised the minority of TH-immunoreactive synapses. Voltammetry demonstrated that DA release was sufficient for the activation of receptors and abolished by blockade of voltage-dependent Na^+ channels or removal of extracellular Ca^{2+}. The lifetime and concentration of extracellular DA was increased by blockade of the DA transporter. Dopamine application depolarized STN neurons, increased their frequency of activity and reduced the impact of γ-aminobutyric acid (GABA)-ergic inputs. These findings suggest that SN DA neurons directly modulate the activity of STN neurons and their loss may contribute to the abnormal activity of STN neurons in PD.

Introduction

The subthalamic nucleus (STN) is a key component of the basal ganglia, a collection of subcortical brain nuclei involved in a variety of motor, associative and limbic functions (reviewed by Wise *et al*., 1996). The STN is also critical for the manifestation of the symptoms that accompany the degeneration of substantia nigra (SN) dopamine (DA) neurons in Parkinson's disease (PD) (reviewed by Bevan *et al*., 2002b). Indeed, the STN is a therapeutic target in PD because interruption of the abnormal pattern and frequency of activity within the nucleus improves motor function (reviewed by Benabid *et al*., 2001). The pathological pattern of activity of the STN in PD is believed to result from the abnormal operation of the striatum that follows the degeneration of the dopaminergic nigrostriatal pathway (reviewed by DeLong, 1990). However, a body of evidence suggests that a direct dopaminergic pathway to the STN may play a role in the operation of the nucleus. (i) A direct dopaminergic projection from midbrain DA neurons to the STN has been identified on the basis of histochemical (Brown *et al*., 1979; Meibach & Katzman, 1979), immunocytochemical (Lavoie *et al*., 1989; Hassani *et al*., 1997; Cossette *et al*., 1999; Hedreen, 1999; Francois *et al*., 2000) and tracing studies (Campbell *et al*., 1985; Hassani *et al*., 1997). (ii) There are pre- and post-synaptic DA receptors in the STN, the activation of which exerts physiological effects (Brown *et al*., 1979; Campbell *et al*., 1985; Mintz *et al*., 1986; Parry *et al*., 1994; Shen & Johnson, 2000; Zhu *et al*., 2002a,b; Baufreton *et al*., 2003; Shen *et al*., 2003; Tofighy *et al*., 2003). (iii) The dopaminergic nigrosubthalamic pathway is subject to degeneration in PD (Francois *et al*., 2000). In spite of this evidence, the role of the dopaminergic nigrosubthalamic pathway remains controversial because, compared with the nigrostriatal pathway, it consists of few fibers and the fibers that are present are thick and non-varicose (Lavoie *et al*., 1989; Cossette *et al*., 1999; Hedreen, 1999; Francois *et al*., 2000). As such, they have been assumed to be fibers of passage and the projection has been thought to exert a relatively minor influence (Lavoie *et al*., 1989; Hedreen, 1999; Smith & Kieval, 2000).

In order to address this issue, we employed correlated light and electron microscopic analysis of tyrosine hydroxylase (TH)-, dopamine β-hydroxylase (DβH)- and DA-immunoreactive elements in the STN to determine whether DA axons in the STN form synaptic contacts. In addition, we employed fast-scan cyclic voltammetry (FCV) at carbon-fibre microelectrodes to determine whether DA is released following the local electrical stimulation of these fibers. The sensitivities of DA release to external Ca^{2+} ion concentration and voltage-dependent Na^+ (Na_v) channel-block and DA transporter (DAT) inhibition were also tested. Finally, perforated patch clamp recording of STN neurons in brain slices was employed to study the

Correspondence: Dr M. D. Bevan, [4]Northwestern University, as above.
E-mail: m-bevan@northwestern.edu

Received 12 May 2004, revised 9 July 2004, accepted 19 July 2004

doi:10.1111/j.1460-9568.2004.03629.x

action of DA, at a concentration similar to that detected by FCV, on autonomous oscillation and GABAergic synaptic transmission/integration, processes that may be critical for patterning STN activity *in vivo* (Bevan *et al*., 2002a,b).

Materials and methods

All procedures involving animals were carried out in accordance with guidelines from institutional Animal Care and Use Committees, the European Communities Council (Directive 86/609/EEC) and the NIH of the USA.

Immunocytochemical detection of TH, DβH and DA in the STN

Neuronal elements in the STN that express TH, DβH and DA were detected using standard immunocytochemical procedures. Fourteen adult Sprague–Dawley rats (Charles River; Wilmington, MA, USA or Margate, Kent, UK), were given a lethal dose of xylazine and ketamine (Sigma-Aldrich) and exsanguinated by transcardial perfusion of phosphate-buffered saline (PBS; 0.01 M PB, pH 7.4) before perfusion with fixative according to the following regimes.

Regime 1

Two animals intended solely for the light microscopic analysis of TH-immunoreactive structures were perfusion-fixed with 500 mL 4% paraformaldehyde (Electron Microscopy Sciences, Fort Washington, PA, USA) in phosphate buffer (PB; 0.1 M, pH 7.4). Following fixation each animal was perfused with 500 mL PB.

Regime 2

Eight animals intended solely for correlated light and electron microscopic analysis of TH-immunoreactive structures were perfusion-fixed with 200 mL 0.1% glutaraldehyde (Electron Microscopy Sciences) and 4% paraformaldehyde in PB followed by 300 mL of the same fixative solution but without glutaraldehyde. Following fixation each animal was perfused with 500 mL PB.

Regime 3

Two animals for the correlated light and electron microscopic analysis of TH- and DβH-immunoreactive structures on alternate sections were perfusion-fixed with 300 mL 0.1% glutaraldehyde and 4% paraformaldehyde in PB followed by 200 mL PB.

Regime 4

Two animals for the correlated light and electron microscopic analysis of DA-immunoreactive structures were perfusion-fixed with 300 mL 5% glutaraldehyde in PB followed by 200 mL PB. Because DA oxidizes readily, the reducing agent sodium metabisulfite (Sigma-Aldrich) was employed at 0.4% in each solution from perfusion until incubation in primary antibodies to DA was complete (Chagnaud *et al*., 1987; Seguela *et al*., 1988). Note that the descending aorta was clamped for regimes 3 and 4, which enabled a reduction in the volume of fixative that was employed. As fixative-containing solutions were perfused over approximately 20–25 min during each regime, flow rates were adjusted accordingly.

Following fixation each brain was removed, cut into blocks and glued to the stage of a vibratome (LeicaVT1000S, Leica Microsystems, Nussloch, Germany), immersed in ice-cold PBS and sectioned in the sagittal or coronal plane at 60 μm. Sections for light microscopic analysis were made more permeable to immunoreagents by the inclusion of the detergent Triton X-100 (0.3%; Sigma-Aldrich) in the solutions containing primary and secondary antibodies. Sections for correlated light and electron microscopic analysis were cryoprotected and then made permeable by a freeze–thaw procedure involving isopentane and liquid nitrogen (see Bolam, 1992). Sections for the light and electron microscope analysis of DA-immunoreactive structures were additionally pretreated with 1% sodium borohydride (Sigma-Aldrich) for 30 min to remove unbound glutaraldehyde.

After at least three washes in PBS, all free-floating sections were incubated in a series of primary, secondary and tertiary antibodies/reagents at 4 °C or room temperature, under gentle agitation. The diluent for these incubations was PBS containing 0.1% bovine serum albumen and 1% normal donkey serum. Sections were first incubated in 1 : 1000 rabbit anti-TH (AB5986P, Chemicon, Temecula, CA, USA) or 1 : 500 monoclonal mouse anti-TH (MAB318, Chemicon or T292, Sigma-Aldrich) or 1 : 500–2000 monoclonal mouse anti-DβH (MAB308, Chemicon) or 1 : 500–2000 rabbit anti-DA (AB122S, Chemicon) for 2–3 days at 4 °C. Following the incubation with primary antibodies, sections were washed three times in PBS and incubated at 4 °C in secondary antibodies overnight. Bound primary antibodies were localized by incubation in a 1 : 100 dilution of biotinylated donkey anti-rabbit or biotinylated donkey anti-mouse IgG (Jackson Immunoresearch, West Grove, PA, USA). Following three washes in PBS, the bound biotinylated secondary antibodies were localized by a 2-h incubation at room temperature in a 1 : 100 dilution of avidin–biotin peroxidase complex (Vector Laboratories, Burlingame, CA, USA). Control incubations in which primary or secondary antisera were omitted were also carried out. Sections were then washed three times in PBS and three times in Tris buffer (50 mM, pH 7.4) before immunoreactive sites were visualized by incubation in Tris buffer containing 0.025% diaminobenzidine tetrahydrochloride (Sigma-Aldrich) and ∼0.001% hydrogen peroxide for 10–20 min. Reactions were terminated by three washes in Tris buffer. Sections were then washed three times in PB, post-fixed in 1% osmium tetroxide (Electron Microscopy Sciences), in PB and dehydrated in a graded series of 50–100% alcohol. To enhance contrast in the electron microscope, sections were stained in 1% uranyl acetate at the 70% alcohol stage. The sections were then treated twice in propylene oxide (Electron Microscopy Sciences), and placed in Durcupan resin (Sigma-Aldrich) overnight. Finally, the sections were embedded in Durcupan resin on microscope slides and cured in an oven for 2 days at 60 °C.

All sections were examined in the light microscope under brightfield illumination (Axioskop, Zeiss) for immunopositive structures. Some of these elements were then drawn and/or captured digitally using a CCD camera (Axiocam, Zeiss), which was operated by the program Axiovision (Zeiss). Sections containing a high density of labelled elements in the STN were then excised and resectioned serially at ∼70 nm (Ultracut E, Leica). Ultrathin sections were stained with lead citrate and viewed and photographed with a Jeol 1200 (Jeol USA, Peabody, MA, USA), a Phillips CM10 (FEI, Hillsboro, OR, USA) or a Zeiss 10B (Zeiss) transmission electron microscope. All immunopositive elements forming synaptic contacts were then photographed and characterized. The diameters of immunoreactive axons and their target structures at sites of synaptic contact were also measured.

Detection of DA release in the STN by FCV

Given that the factors influencing the release and lifetime of DA *in vivo* and *in vitro* are similar (e.g. Jones *et al*., 1995; Schmitz *et al*.,

2003), we studied the release of DA in the STN in brain slices because advantages of this preparation include the precise placement of stimulation and carbon-fibre recording electrodes under visual guidance and the ability to control the local chemical environment through the bath application of drugs and artificial cerebrospinal fluid (ACSF).

Nine adult Sprague–Dawley rats (Charles River, UK) were killed by an overdose of halothane. The brain was removed rapidly, blocked along the midline, and each hemisphere glued to the stage of a vibratome (VT 1000S, Leica). Sagittal slices containing the STN and striatum were cut at a thickness of 350–400 μm in ice-cold, HEPES-buffered ACSF saturated with 95% O_2/5% CO_2, which contained (in mM): 120 NaCl, 20 $NaHCO_3$, 6.7 HEPES acid, 3.3 HEPES salt, 5 KCl, 2 $CaCl_2$, 2 $MgSO_4$ and 10 glucose, as used previously (Cragg *et al*., 1997a). Prior to recording, slices were maintained at room temperature (~20–25 °C) in a holding chamber containing HEPES-ACSF, which was bubbled continuously with 95% O_2/5% CO_2. Slices were held in this chamber for at least 1 h. Upon transfer to a recording chamber, slices were superfused continuously (1.5 mL/min) with bicarbonate-buffered ACSF (95% O_2/5% CO_2) at 32 °C containing (in mM): 124 NaCl, 26 $NaHCO_3$, 3.7 KCl, 1.3 $MgSO_4$, 1.3 KH_2PO_4, 10 glucose and 2.4 $CaCl_2$ (unless otherwise indicated), as described previously (Cragg *et al*., 1997b). Slices were equilibrated in the recording chamber for at least 30 min prior to recording. A ×10 water-immersion objective (Olympus, Tokyo, Japan) was used to locate the STN within each slice.

Extracellular DA concentration ($[DA]_o$) was monitored using FCV with 6–8 μm carbon-fibre microelectrodes beveled to a point (exposed tip length, ~30 μm; MPB Electrodes, London, UK) and a Millar Voltammeter (PD Systems, West Molesey, UK) (Cragg & Greenfield, 1997; Cragg, 2003) at a sample rate 4–8 Hz. The applied waveform was a dual-triangular waveform scanning from −0.7 V to 1.3 V to −0.7 V vs. Ag/AgCl at a scan rate of 800 V/s. Illustrated voltammograms are currents obtained after digital subtraction of background current. Identification of the released substance as DA required that monitored voltammograms contained current peaks for oxidation and reduction at potentials (+550 and −200 mV vs. Ag/AgCl, respectively) that matched those of exogenous DA in solution. Electrodes were calibrated in 1–2 μM DA, norepinephrine (NE) and 5-HT in experimental media. The detection limit for $[DA]_o$ (~2 × noise) was ~10–50 nM.

Neurotransmitter release was evoked by local stimulation (DS3 Isolated Stimulator, Digitimer Ltd, Welwyn Garden City, UK) at surface bipolar electrodes 50 μm apart (Cragg & Greenfield, 1997; Cragg, 2003). Stimulus pulses (200 μs width) were applied at perimaximal current (0.55–0.8 mA) locally to the STN at a distance from the recording electrode of ~100 μm, either as single pulses, or in trains of 50 pulses at 50 Hz. Perimaximal stimulation current was optimized for single pulse-evoked DA release in the striatum and was also employed in the STN to minimize the variability of release due to stimulation failure. In experiments designed to test the Na_v channel- and Ca^{2+}-sensitivity of evoked release, the DA uptake inhibitor GBR 12909 (500 nM; RBI, Natick, MA, USA) was bath-applied continuously to maximize the identification, detection and ratio of $[DA]_o$ signal to noise. Where measurements at a given recording site were made prior to, during and after a treatment, stimuli were repeated at intervals of a minimum of 10 min, after which time release was restored to pretreatment levels (data not illustrated).

Voltammetric data were acquired and analysed using Strathclyde Whole Cell Program (University of Strathclyde, Glasgow, UK). Data are given as mean ± SD and sample size, *n*, represents the number of recording sites. Data were analysed using GraphPad Prism (GraphPad Software, San Diego, CA, USA). Comparisons for differences in means were assessed by unpaired (Mann–Whitney *U*-tests, M-WU) or paired (Wilcoxon signed-rank, WSR) non-parametric tests.

Electrophysiological recording of the action of exogenous DA on STN neurons

Electrophysiological studies were performed on brain slices prepared from six 16- to 25-day-old Sprague–Dawley rats (Charles River). Animals were deeply anaesthetized with a mixture of ketamine and xylazine and perfused transcardially with 10–40 mL ice-cold modified ACSF, which had been bubbled with 95% O_2/5% CO_2 and contained (in mM): 230 sucrose, 26 $NaHCO_3$, 2.5 KCl, 1.25 Na_2HPO_4, 0.5 $CaCl_2$, 10 $MgSO_4$, and 10 glucose. The brain was then rapidly removed, blocked in the sagittal/parasagittal plane, glued to the stage of a vibratome (3000 Deluxe; Technical Products International, St Louis, MO, USA), and immersed in ice-cold modified ACSF. Slices containing the STN were cut at a thickness of 300 μm and subsequently transferred to a holding chamber, where they were submerged in ACSF, which was bubbled continuously with 95% O_2/5% CO_2, maintained at room temperature, and contained (in mM): 126 NaCl, 26 $NaHCO_3$, 2.5 KCl, 1.25 Na_2HPO_4, 2 $CaCl_2$, 2 $MgSO_4$, and 10 glucose.

Single slices were transferred to the recording chamber and perfused continuously (2–3 mL/min) with oxygenated ACSF at 37 °C. Somatic recordings were made using patch pipettes pulled from standard-wall borosilicate glass (Warner Instrument Co., Hamden, CT, USA) on a P-97 Flaming/Brown micropipette puller (Sutter Instrument Co., Novaton, CA, USA). Pipettes were filled with a solution containing (in mM): 110 K-$MeSO_4$, 25 KCl, 3.6 NaCl, 1 $MgCl_2.6H_2O$, 10 HEPES, 0.1 Na_4EGTA, 0.4 Na_3GTP, and 2 $Mg_{1.5}ATP$. The pH and osmolarity of the pipette solution were 7.3 and 290 mOsm, respectively. Gramicidin was added to the pipette solution at an approximate concentration of 15 μg/mL less than 1 h before seal formation was attempted. The resistance of filled pipettes was between 2.5 and 5.0 MΩ. Gramicidin was employed as the pore-forming agent in perforated patch recordings because it forms pores that are permeable only to monovalent cations and small neutral molecules such as water. This technique therefore preserves the intrinsic physiological properties of STN neurons including the intracellular transduction pathways that are activated by DA, the gradient of anions that permeate GABA-A receptors and intrinsic calcium dynamics, which regulate firing (Myers & Haydon, 1972; Abe *et al*., 1994; Kyrozis & Reichling, 1995; Bevan *et al*., 2000, 2002a; Hallworth *et al*., 2003). A 40× water-immersion objective (Axioskop, Zeiss) was used to examine each slice using infragradient contrast video microscopy (Dodt *et al*., 1999; Infrapatch Workstation; Luigs and Neumann, Ratingen, Germany). Perforated recordings were made in current-clamp mode using an Axopatch 200B amplifier (Axon Instruments, Union City, CA, USA) that was operated using Axograph 4 software (Axon Instruments). Signals were low-pass filtered at 10 kHz and digitized at 50 kHz. Deliberate or accidental establishment of the whole-cell configuration was recognized as a sudden drop in series resistance, an increase in the amplitude of recorded action potentials, a depolarizing shift in the equilibrium potential of the evoked GABA-A inhibitory post-synaptic potential (IPSP; Bevan *et al*., 2000, 2002a) and a +5 mV offset in membrane potential. The latter was measured as an increase in the threshold for the generation of action potentials that accompanied break-in. The value of the offset was smaller than the empirically calculated junction potential between the electrode solution and the external media of ~+9 mV (Neher, 1992; Barry, 1994). The recorded voltage was therefore ~4 mV more depolarized than the true voltage

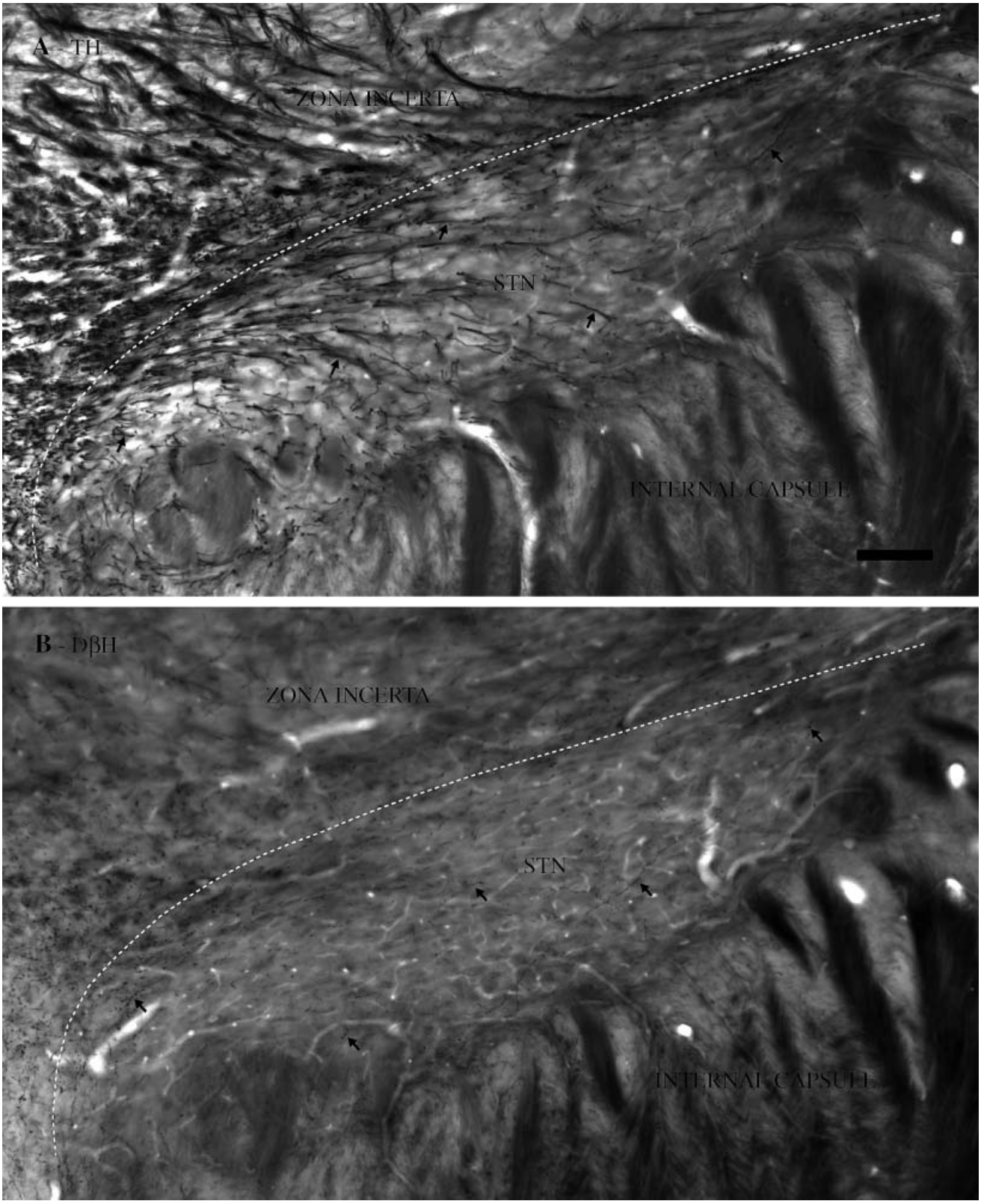

FIG. 1. The STN is innervated by numerous TH-immunoreactive axons. Light micrographs of TH- and DβH-immunoreactivity at the surface of adjacent coronal sections of the STN. Medial is to the left and lateral is to the right. (A) In this low-magnification micrograph of a coronal section from the middle third (along the rostral–caudal axis) of the STN (dorsal boundary delineated by the dotted line), numerous TH-immunoreactive axons/axon bundles (some indicated by arrows) can be observed to course along a largely medial–lateral axis. (B) In the adjacent section of the STN (dorsal boundary delineated by the dotted line), a smaller number of fine DβH-immunoreactive axons (some indicated by arrows) may be noted. In general, the appearance and trajectory of these axons is distinct from the majority of those labeled with TH (see also Fig. 2). Scale bar in A, 100 μm (A and B).

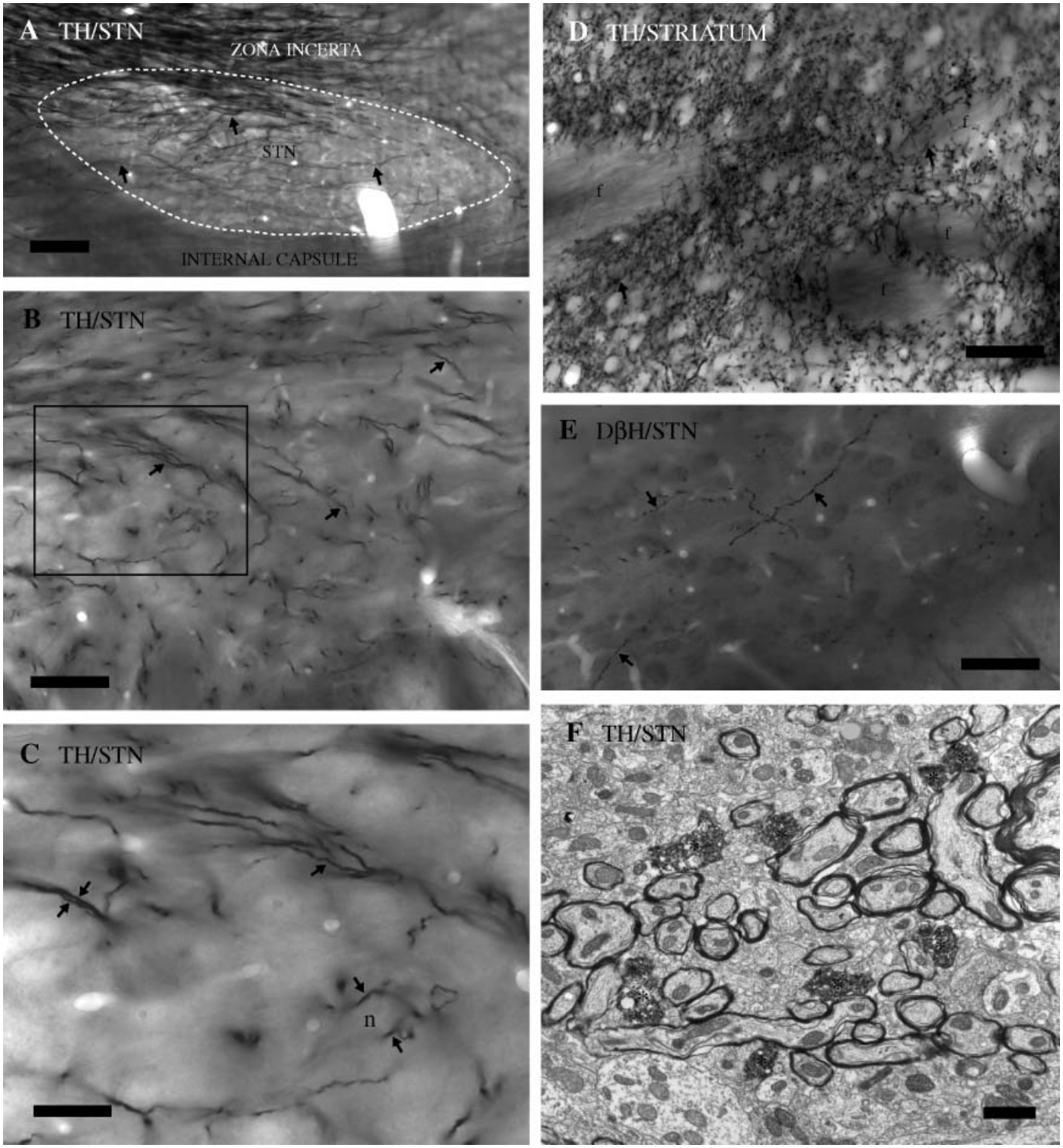

FIG. 2. The STN is innervated by numerous TH-immunoreactive axons. (A) In this low-magnification micrograph of the surface of a sagittal section from the medial third (along the medial–lateral axis) of the STN (boundary delineated by the dotted line), numerous TH-immunoreactive axons/axon bundles (some indicated by arrows) can be observed to course along a largely rostral–caudal axis. Rostral is to the left and caudal is to the right in this micrograph. (B) High-magnification micrograph of numerous TH-immunoreactive axons/axon bundles from the section illustrated in A (some indicated by arrows). The area within the rectangular box in B is displayed at 2.5× higher magnification in C. Note that immunoreactive axons (arrows) are tightly or loosely arranged in bundles and in some cases appear to contact the soma of an unlabeled STN neuron (n). (D) Micrograph of TH-immunoreactivity in the striatum. For comparison, the micrograph was taken at the same magnification and from the same section as that illustrated in Fig. 1B. Note the greater density, finer caliber, more tortuous course and relatively varicose nature of TH-immunoreactive fibers (some indicated by arrows) in the striatum. The immunoreactive neuropil is penetrated by non-immunoreactive fibre bundles (f). (E) High-magnification micrograph of DβH-immunoreactive fibers from the section illustrated in B. Note the relatively low-density, fine-caliber and varicose nature compared with the majority of TH-immunoreactive fibers from an adjacent section in B and C. (F) Electron micrograph of TH-immunoreactive axons (asterisks) in the STN. As TH-immunoreactive axons in the STN often occur in bundles it is likely that some of the thicker labeled fibers in light micrographs in fact comprised multiple labeled axons that were in close proximity to each other. Scale bars, 100 μm (A); 50 μm (B, D and E); 20 μm (C); 1 μm (F).

and was corrected accordingly off-line. Fast capacitive transients due to the pipette and voltage errors attributable to series resistance were nulled on-line.

N-methyl-D-aspartic acid (NMDA), α-amino-3-hydroxy-5-methyl-4-isoxazolepropionic-acid (AMPA) and GABA-B receptors were blocked by the continuous bath-application of 50 μM D-(–)-2-amino-5-phosphonopentanoic acid (APV), 20 μM 6,7-dinitroquinoxaline-2,3-dione (DNQX) and 1 μM CGP 55845, respectively, so that the actions of DA on synaptic transmission involving those receptors could be excluded and stimulated GABA-A IPSPs could be studied in isolation. GABA-A IPSPs were elicited by bipolar electrical stimulation (A360 stimulus isolator; World Precision Instruments, Sarasota, FL, USA) of the internal capsule rostral to the STN. The poles of stimulation were selected from a custom-built matrix of 20 stimulation electrodes (MX54CBWMB1; FHC, Maine, ME, USA). The matrix comprised four rows of electrodes with five electrodes in each row. The tip of each electrode was separated from the tip of the nearest neighbouring electrode by approximately 200 μm. The shank and tip of each electrode was approximately 125 μm and 10 μm in diameter, respectively. The impedance of each electrode was 50–100 kΩ. The two electrodes selected for stimulation were those that produced the largest IPSP in the absence of antidromic activation. Supramaximal stimulation was employed so that failure to stimulate GABAergic fibers would contribute little to the variability of the observed responses. Thus stimulation intensity (0.05–0.5 mA) was increased to generate the largest IPSP possible and then increased further by approximately 20%. The duration of stimulation was 0.1–0.2 ms. The selective GABA-A antagonist, SR 95531 hydrobromide (GABAzine; 20 μM) was bath-applied in several cases to further verify that the evoked IPSP was due solely to GABA-A receptor activation.

In order to study the effects of DA on autonomous oscillation and inhibitory synaptic integration, single GABA-A IPSPs were evoked at 10 s intervals or greater under control conditions and in the presence of 1 μM DA during autonomous oscillation. Dopamine was prepared immediately prior to each experiment, in the presence of 50 μM sodium metabisulfite and applied under reduced light to impair oxidation. Synaptic transmission receptor blockers were obtained from Tocris (Ellisville, MO, USA) and DA was obtained from Sigma-Aldrich.

The effects of DA on the autonomous activity and the magnitude and integral of evoked GABA-A IPSPs (GABA-A $IPSP_{mag}$ and GABA-A $IPSP_{int}$, respectively) in STN neurons were analysed using Axograph 4 (Axon) and Origin 6 (Microcal, Northampton, MA, USA). Descriptive statistics refer to the mean ± SD. The means of

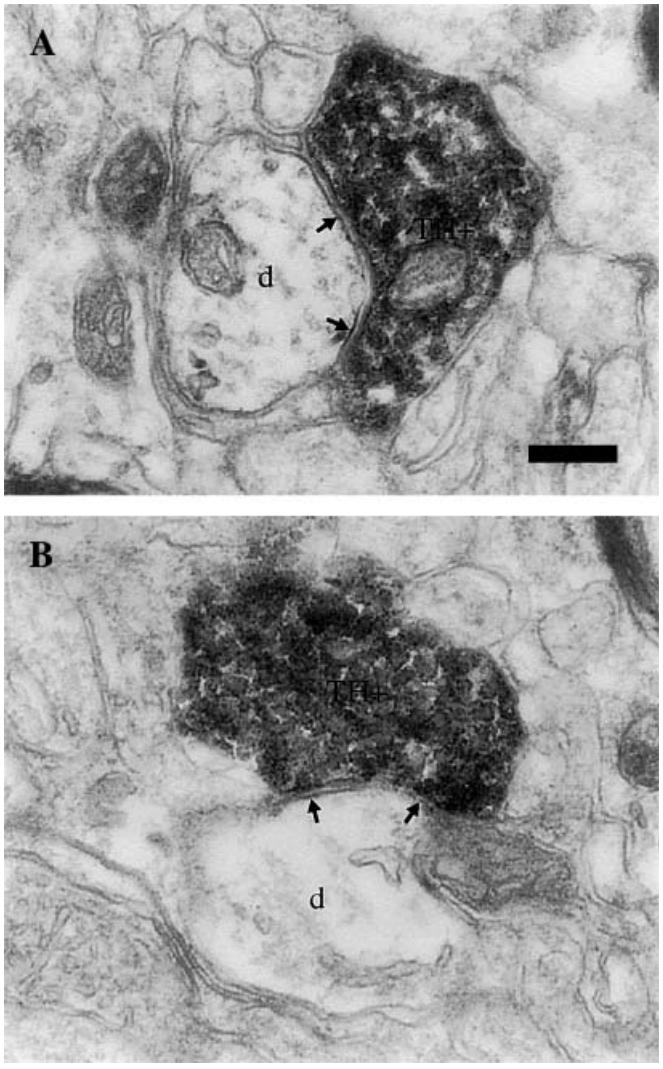

FIG. 3. TH-immunoreactive axons predominantly form symmetric synaptic contacts with the small-diameter dendrites of STN neurons. (A and B) Two examples of TH-immunoreactive (TH+) axons that formed symmetric synaptic contacts (arrows) with the small diameter dendrites (d) of STN neurons. Scale bar in A, 0.2 μm (A and B).

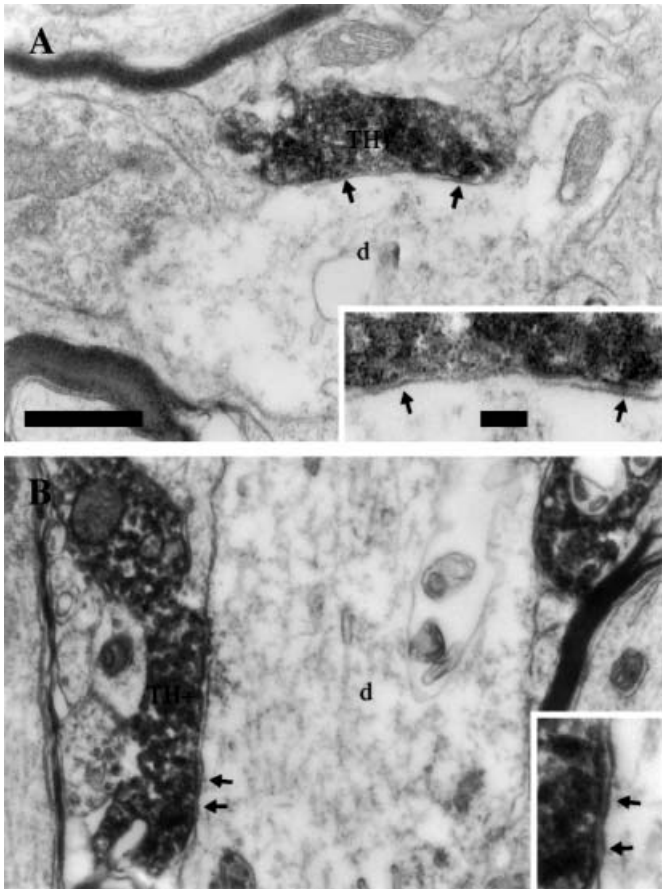

FIG. 4. TH-immunoreactive axons also form symmetric synaptic contacts with the large diameter dendrites of STN neurons. (A and B) Two examples of TH-immunoreactive (TH+) axons that formed symmetric synaptic contacts (arrows) with the large-diameter (> 1 μm) dendrites (d) of STN neurons. Scale bars (A also applies to B), 0.5 μm (main panel) and 0.1 μm (insets).

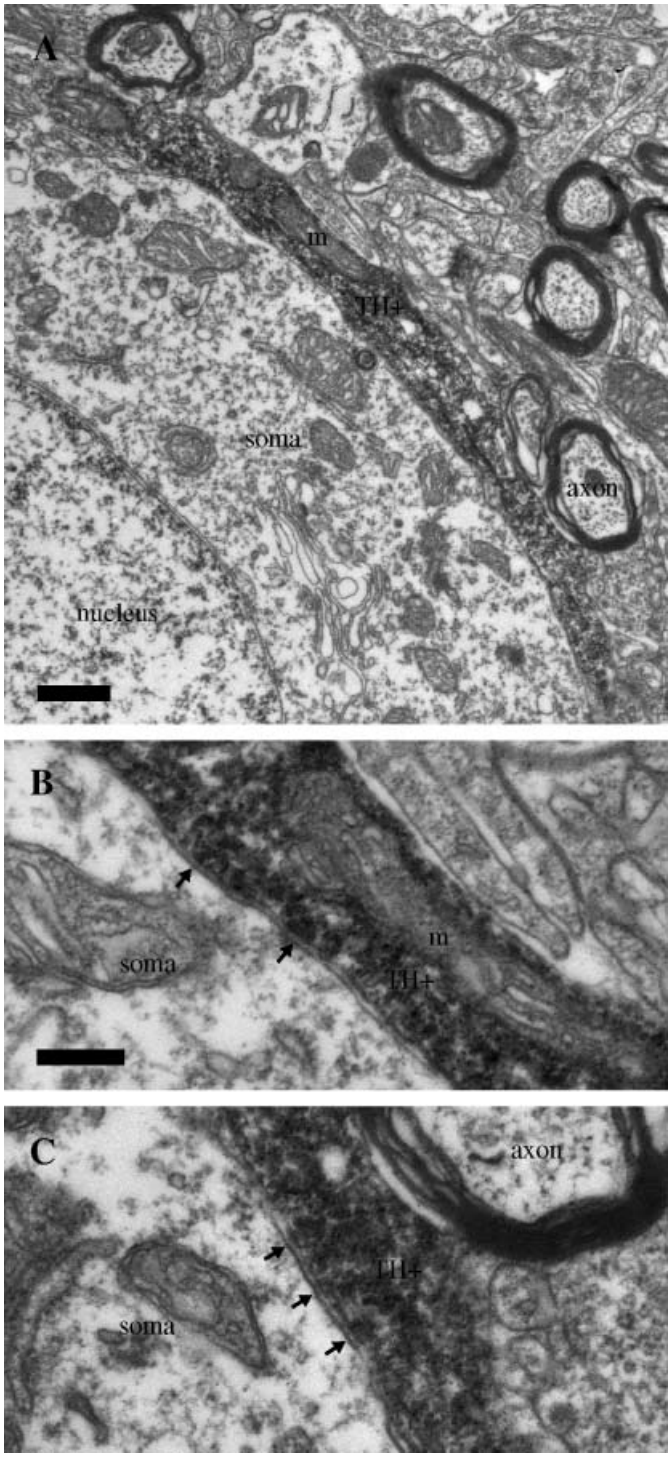

FIG. 5. TH-immunoreactive axons also form symmetric synaptic contacts with the somata of a subpopulation of STN neurons. (A–C) An example of a TH-immunoreactive (TH+) axon that established multiple, symmetric synaptic contacts (arrows) with the somata of an STN neuron. The labeled axon in A coursed along the soma of an STN neuron and possessed several active zones that are shown at higher magnification in B and C. A large mitochondrion (m) within the labeled axon and an unlabeled, myelinated axon serve as registration points for the low- (A) and high-magnification micrographs (B and C). Scale bar, 0.5 μm (A); scale bar in B, 0.2 μm (B and C).

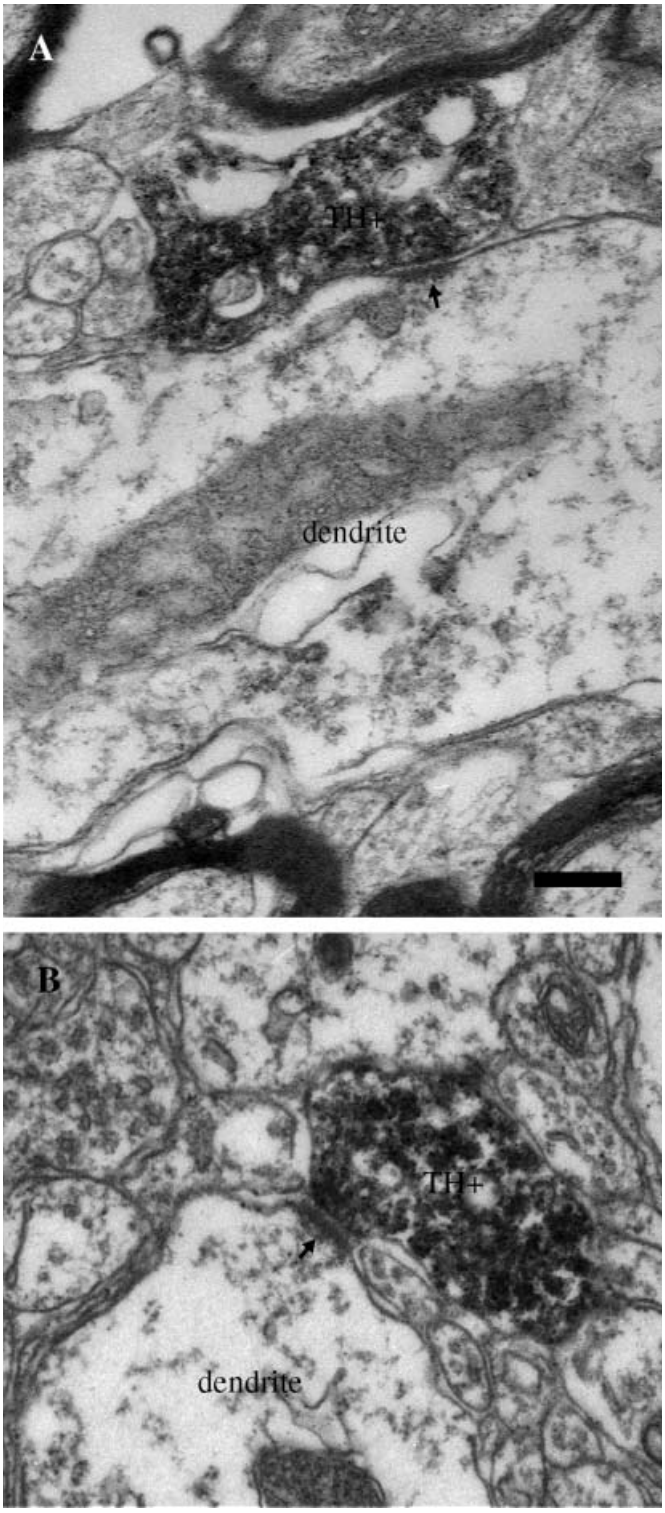

FIG. 6. A minority of TH-immunoreactive axons form asymmetric synaptic contacts with STN neurons. (A and B) Two examples of TH-immunoreactive (TH+) axons that formed asymmetric synaptic contacts (arrows) with the dendrites of STN neurons. Note the relatively thick post-synaptic specializations and wide synaptic clefts compared with the TH-immunoreactive symmetrical synaptic junctions in Figs 3–5. Scale bar in A, 0.2 μm (A and B).

TABLE 1. Morphological properties and synaptic targets of TH-, DβH- and DA-immunoreactive axons in the STN

Antigen	Type of synapse	*n*	Diameter of axon (μm)	Post-synaptic targets		
				Soma	Dendrite > 1 μm	Dendrite < 1 μm
TH	Symmetric	122	0.40 ± 0.14	18	28	76
TH	Asymmetric	18	0.43 ± 0.14	0	6	12
DβH	Asymmetric	12	0.34 ± 0.14	0	11	1
DA	Symmetric	21	0.35 ± 0.12	1	4	16
DA	Asymmetric	5	0.35 ± 0.09	0	1	4

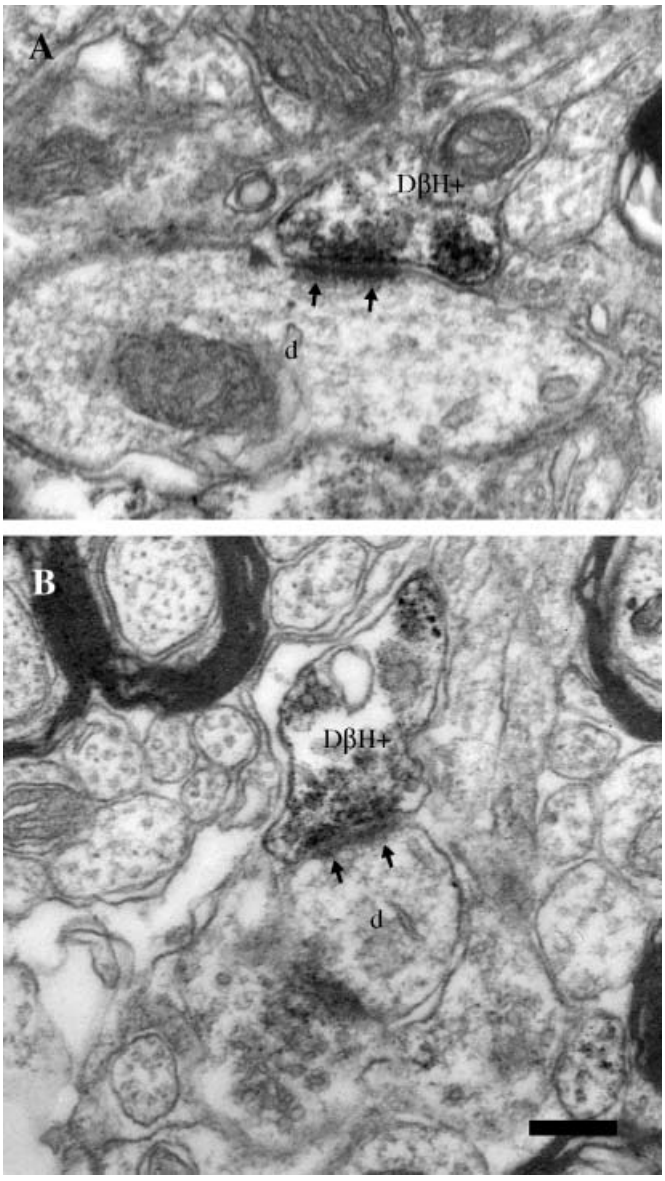

FIG. 7. DβH-immunoreactive axons form asymmetric synaptic contacts with the dendrites of STN neurons. (A and B) Two examples of DβH-immunoreactive (DβH+) axons that formed asymmetric synaptic contacts (arrows) with the dendrites (d) of STN neurons. In this material, the DAB immunoreaction product was less homogeneously distributed throughout the axon than the reaction product formed during TH immunocytochemistry. Note the relatively thick post-synaptic specializations and wide synaptic clefts compared with the TH-immunoreactive symmetric synaptic junctions in Figs 3–5. Scale bar in B, 0.2 μm (A and B).

paired experimental datasets were compared using the WSR test and probability values < 0.05 were considered significant.

Results

TH-, DβH- and DA-immunoreactive elements in the STN

Light microscopic observations

Immunoreactive elements were filled with the dark brown, amorphous reaction product that is characteristically formed when DAB is used as the chromogen for the peroxidase reaction. Labeling was absent when primary or secondary antisera were omitted from immunocytochemical incubations.

In line with previous observations, the STN contained TH-immunoreactive axons (Figs 1A and 2A–C; Campbell *et al*., 1985; Lavoie *et al*., 1989; Hassani *et al*., 1997; Cossette *et al*., 1999; Hedreen, 1999; Francois *et al*., 2000). The pattern of labelling was similar in the paraformaldehyde and paraformaldehyde/glutaraldehyde perfusion-fixed tissue. The number of fibers and the density and depth of labeling was clearly greater in tissue that been treated with detergent, presumably due to the better penetration of immunoreagents and greater access of antibodies to the TH antigen (Bolam, 1992). The pattern of labeling was indistinguishable when either polyclonal or monoclonal antibodies were employed to detect TH.

Within single sections, individual TH-immunoreactive axons/axon bundles were observed to extend for large distances along the dorsal–ventral and/or medial–lateral and/or caudal–rostral axes of the STN (Figs 1A and 2A). Such fibers therefore possessed the potential to influence large numbers of STN neurons in different sectors of the nucleus. Examination at high magnification of thick immunoreactive 'fibers' revealed that some were, in fact, composed of multiple, smaller diameter axons (Fig. 2B and C). Indeed, individual axons were often seen to detach from the parent fibre bundle and pursue an independent but similarly linear course through the nucleus. Single immunoreactive axons were typically cable-like structures with few or very slender varicose regions (Fig. 2B and C). Only a small proportion of STN neuronal somata were apposed by immunoreactive axons (e.g. Fig. 2C), even in tissue that was prepared solely for light microscopy and was therefore optimal for the detection of TH-immunoreactive elements and contained TH-immunoreactive elements throughout the thickness of each section.

The appearance of TH-immunoreactive axons in the STN was compared with the appearance of immunoreactive axons in the striatum from the same sagittal section. As described previously, the striatum was associated with a far greater density of labeled axons (cf. Fig. 2B and D; Lavoie *et al*., 1989; Hassani *et al*., 1997; Cossette *et al*., 1999; Hedreen, 1999). Furthermore, immunoreactive axons in the striatum gave rise to more elaborate terminal arborizations (cf. Fig. 2B and D; see reviews by Smith & Bolam, 1990; Sesack, 2002).

TH is an enzyme that is utilized by both DA- and NE-releasing axons, whereas DβH is an enzyme that is utilized in the synthesis of NE but not DA. Therefore, in two animals, the appearance and density of TH-immunoreactive and DβH-immunoreactive fibers in the STN were compared on alternate detergent-treated sections to determine, in a qualitative manner, the relative contribution of NE-releasing axons to the population of axons labeled by TH. The density of DβH-immunoreactive fibers in the STN was clearly lower than the density of TH-immunopositive fibers on adjacent sections (cf. Figs 1A and B, and 2B and E). Although this observation could result from the relative insensitivity of the DβH antibody compared with the TH antibody that was employed, dense DβH labeling was observed in regions with a well-characterized innervation by NE fibers (not

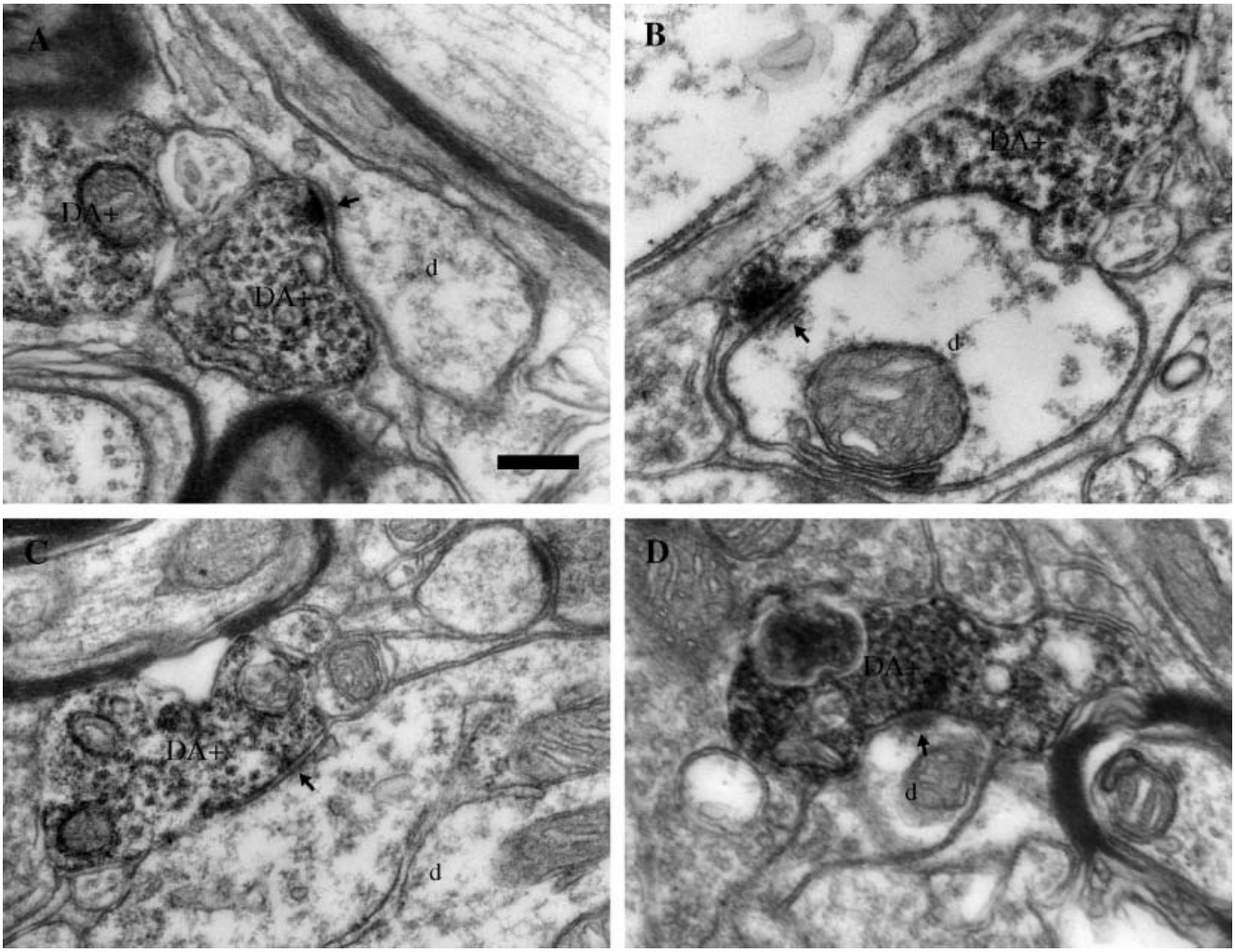

FIG. 8. DA-immunoreactive axons predominantly form symmetric synaptic contacts with STN neurons. Examples of DA-immunoreactive (DA+) axons that formed synaptic contacts (arrows) with STN neurons. The relatively low density of DAB reaction product in the 5% glutaraldehyde fixed tissue allows synaptic vesicles and the association of these vesicles with synapses to be seen with greater clarity. (A and B) Two examples of synaptic contacts with small-diameter dendrites (d). (C) A DA-immunoreactive axon in synaptic contact with a proximal dendrite (d; the full extent of the dendrite is not shown). (D) A rarer example of a DA-immunoreactive (DA+) axon that formed an asymmetric synaptic contact (arrow) with a small-diameter dendrite (d) of a STN neuron. Scale bar in A, 0.2 μm (A and B–D).

illustrated), e.g. the substantia innominata (Chang, 1989), the cortex (Seguela *et al*., 1990), the reticular thalamic nucleus (Asanuma, 1992) and the amygdala (Asan, 1993). DβH-immunoreactive fibers also appeared finer and more varicose than the majority of TH-immunopositive fibers/fiber bundles, suggesting that the majority of TH fibers do not release a catecholamine other than DA (compare Fig. 2B and E). This deduction is further supported by ultrastructual evidence that will be presented in the next section that DβH-immunoreactive axons exhibit synaptic specializations that are distinct from the majority of those associated with TH-immunoreactive axons.

Dopamine-immunoreactive axons were relatively sparse in the STN, even in detergent-treated sections. Immunoreactivity was confined to the uppermost 2–5 μm of each section. The sparsity of DA-immunoreactive axons is likely to be a technical artifact. The high concentration of glutaraladehyde fixative that was employed is well known to restrict the access of antibodies to antigenic sites (Bolam, 1992). Furthermore, DA is relatively ephemeral in nature compared with enzymes such as TH and DβH because it is readily oxidized and released from synaptic terminals (Chagnaud *et al*., 1987).

Electron microscopic observations

At the electron microscopic level, TH-, DβH- and DA-immunoreactive axons contained an amorphous, flocculent, electron-dense DAB reaction product that adhered to subcellular organelles and plasma membranes. Labeling was often so dense in TH-immunostained sections that the detailed morphology of subcellular organelles was obscured. Tyrosine hydroxylase-immunoreactive axons varied considerably in their diameter but were invariably unmyelinated. In line with light microscopic observations, labeled axons often occurred in small groups or bundles (Fig. 2F). Immunoreactive axons typically contained vesicles, microtubules and mitochondria (Figs 3–6). Immunoreactive axons predominantly formed symmetric synaptic contacts (Figs 3–5, Table 1) that were characterized by symmetric membrane specializations, parallel pre- and post-synaptic membranes and the association and/or docking of synaptic vesicles with presynaptic membrane specializations. In line with reports from other brain regions, TH-immunoreactive symmetric synapses often exhibited only a slightly widened spacing of pre- and post-synaptic membranes

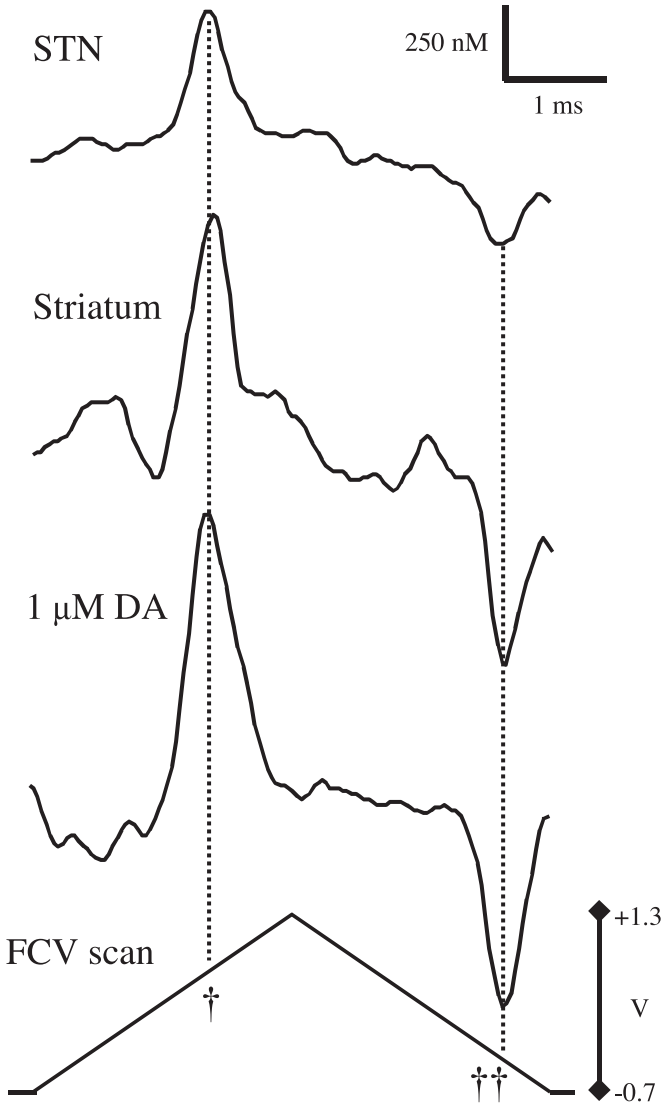

FIG. 9. Local electrical stimulation evokes the release of DA in the STN. Examples of individual voltammograms obtained after local electrical stimulation of the STN and dorsal striatum and in a 1 μM solution of DA in ACSF, plotted against the FCV scan. Peak oxidation (†) and reduction (††) potentials for DA (approximately +0.6 V and −0.25 V, respectively, vs. Ag/AgCl) are indicated (dotted lines). Protocols for stimulation pulses (200 μs, 0.5 mA): STN, 50 pulses at 50 Hz in the presence of GBR 12909 (500 nM); striatum, one pulse.

(Sesack, 2002). Another helpful feature that was used to identify TH-immunoreactive symmetric synapses was the consistent occurrence of electron-dense cleft material at sites of putative synaptic contact (Figs 3–5). In agreement with our light microscopic observations and previous studies on DA axons, the caliber of TH-immunoreactive axons did not vary much and synapses often occurred along the non-varicose sections of the axons (e.g. Fig. 5). The vesicles in proximity to synaptic zones were similar in appearance and dimensions to the vesicles throughout each axon (Figs 3–5).

TH-immunoreactive axons predominantly formed symmetric synaptic contacts with the dendrites of STN neurons, including small- (Fig. 3, Table 1), medium- and large- (Fig. 4, Table 1) diameter dendrites and dendritic spines (not illustrated). A smaller proportion of immunoreactive axons formed symmetric synapses with the somata of STN neurons (Fig. 5, Table 1) but even in the areas of strongest labeling, only a minority of STN neuronal somata received synaptic inputs from immunoreactive axons. Occasionally, individual axons formed multiple, symmetric synaptic contacts with single post-synaptic dendrites or soma (e.g. Figs 3A and B, 4B and 5).

A small proportion of TH-immunoreactive axons formed asymmetric synapses (Fig. 6, Table 1). These synapses typically possessed more distinct synaptic clefts and a thicker post-synaptic membrane specialization than TH-immunoreactive symmetric synapses. Each asymmetric synaptic contact was made with the dendrite of an STN neuron.

Axons that were DβH-immunoreactive were unmyelinated and formed asymmetric axodendritic synaptic contacts with STN neurons (Fig. 7, Table 1). This observation provides further evidence that the majority of symmetric TH-immunoreactive synaptic contacts in the STN are not formed by NE-releasing axons. Norepinephrinergic axons form asymmetric (Chang, 1989; Asanuma, 1992), symmetric (e.g. Seguela *et al*., 1990) or a combination of asymmetric and symmetric (Asan, 1993) synapses in other brain regions.

Dopamine-immunoreactive axons were similar in morphology to those immunoreactive for TH, i.e. they were unmyelinated and the majority of synaptic contacts were symmetric, predominantly formed with dendrites (Fig. 8A–C, Table 1) and occasionally with somata (Table 1) of STN neurons. The predominantly symmetric nature of DA-immunoreactive synaptic terminals has also been reported for the striatum (Descarries *et al*., 1996; Karle *et al*., 1996), nucleus accumbens (Voorn *et al*., 1986) and cerebral cortex (Seguela *et al*., 1988). The better preservation of the DA-immunoreactive material and the lower density of DAB reaction product (due presumably to the high concentration of glutaraldehyde that was employed during perfusion-fixation) enabled to us identify and demonstrate symmetric synapses more easily than in TH-immunoreactive material. As in other brain regions (Voorn *et al*., 1986; Seguela *et al*., 1988; Karle *et al*., 1996) a minority of DA-immunoreactive axons formed asymmetric axodendritic contacts (Fig. 8D, Table 1). Whether these are DA-releasing axons and/or NE-releasing axons, in which DA is a precursor for the production of NE remains to be determined.

Detection of DA release in the STN

The release of a monoamine-like substance in the STN was detected using FCV at carbon-fibre microelectrodes following local electrical stimulation (50 Hz, 50 pulses). Voltammograms of the released substance were readily attributable to a monoamine: oxidation and reduction peak potentials (∼ 600 mV and ∼−200 mV, respectively, vs. Ag/AgCl) were identical to those detected for DA in solution and for DA signals evoked in dorsal striatum (Fig. 9).

Recording sites in the STN were selected randomly. Release of a DA-like substance at concentrations greater than 50 nM were observed at about half (17/32) of the recording sites. This result is consistent with the discrete distribution of dopaminergic fibers in the STN and the discrete spatial resolution of the carbon-fiber recording microelectrode. The restricted loci for release were in contrast to the release of DA at all randomly selected sites (see Cragg, 2003) in the more densely and homogeneously innervated dorsal striatum. The peak $[DA]_o$ that was released in the STN following local stimulation (50 Hz, 50 pulses) ranged from 100 to 500 nM (Fig. 9; without uptake inhibition). These concentrations are less than the typical peak $[DA]_o$ that was evoked by single pulses in the dorsal striatum (e.g. Fig. 9; Cragg *et al*., 1998).

Dopamine was not the only electroactive amine detected in the STN; the release of a substance identified as the indoleamine, 5-hydroxytryptamine (5-HT; peak potentials: oxidation, ∼+600 mV;

double reduction, −50 mV and −600 mV; see Cragg *et al.*, 1997a), was also detected occasionally (5/32 recording sites) at concentrations equivalent to 50–100 nM 5-HT (not illustrated). Sites with detectable 5-HT release were excluded from further study so that the release of DA could be studied in isolation.

Roles of the DA transporter, Na_v channels and $[Ca^{2+}]_o$ in DA availability

The extracellular lifetime of DA that was released following 50 Hz, 50 pulse stimulation was markedly extended by competitive inhibition of the DAT with GBR 12909 (500 nM; Fig. 10A). Moreover, the mean peak $[DA]_o$ was significantly greater in the presence of GBR 12909 (330 ± 130 nM) than in control (190 ± 55 nM; Fig. 10A; $P < 0.05$, M-WU test, $n = 5$ in control media and $n = 8$ in GBR12909, unpaired observations). These data not only suggest that the extracellular availability of DA in the STN is regulated by the DAT but also support the view that the substance measured is predominantly DA, and not the monoamine NE. Because inhibition of the DAT does not inhibit DA release, these data also eliminate the reversal of the DAT (e.g. Levi & Raiteri, 1993; Sulzer *et al.*, 1995; Falkenburger *et al.*, 2001) as a mechanism for DA release in the STN.

For the optimal positive detection and identification of DA in the STN, all subsequent experiments were conducted in the presence of GBR 12909 (500 nM). Blockade of Na_v channels with 1 μM tetrodotoxin (TTX, Tocris) rapidly abolished the release of DA evoked by 50 Hz, 50 pulse stimulation in the STN (Fig. 10B; peak concentration detected was 5 ± 26% of control; $P < 0.05$, WSR test, $n = 6$). Furthermore, evoked DA release was abolished when external Ca^{2+} was removed from the media (Fig. 10C; peak concentration 4 ± 8% of control; $P < 0.05$, WSR test, $n = 6$), and recovered to control levels when external Ca^{2+} was returned to its normal concentration (Fig. 10C; peak concentration 84 ± 12% of control; $P > 0.05$, WSR test, $n = 6$).

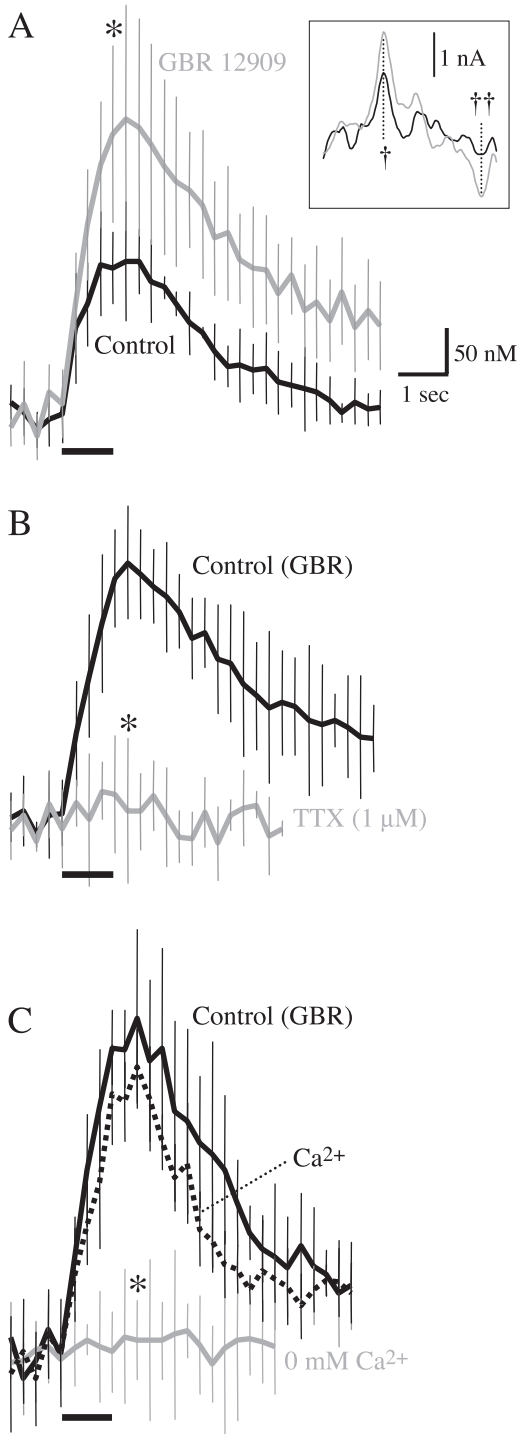

FIG. 10. The profile of extracellular DA in the STN is modulated by the DAT and release of DA is sensitive to Na_v channel-block and external $[Ca^{2+}]$. (A) Mean $[DA]_o$ ± SD vs. time detected in response to 50 pulse (*p*), 50 Hz stimulation (solid bar) in control (untreated, black line) and in the presence of the DA uptake inhibitor, GBR 12909 (500 nM; grey line). The lifetime of extracellular DA and the mean peak $[DA]_o$ are increased in GBR 12909 compared with control conditions ($P < 0.05$, M-WU test, $n = 5$ in control media and $n = 8$ in GBR 12909 containing media), confirming that the released monoamine is DA. Inset: averages of representative voltammograms obtained in control conditions (black) and in the presence of GBR 12909 (grey). Peak potentials are indicated (dotted lines) for DA oxidation (†) and reduction (††). (B) Mean $[DA]_o$ ± SD vs. time detected in response to 50 pulse, 50 Hz stimulation in control (black line) and in the presence of 1 μM TTX. Blockade of Na_v channels with TTX abolished the evoked release of DA ($P < 0.05$, WSR test, $n = 6$). GBR 12909 (500 nM) was present throughout. (C) Mean $[DA]_o$ ± SD vs. time detected in response to 50 pulse, 50 Hz stimulation in control (black line, 2.4 mM Ca^{2+}), during 0 mM Ca^{2+} (grey line) and on return to 2.4 mM Ca^{2+} (dashed line). The release of DA was largely abolished when Ca^{2+} was removed from the external media ($P < 0.05$, WSR test, $n = 6$) but recovered when external Ca^{2+} was returned to normal levels. GBR 12909 (500 nM) was present throughout. Sample rate was 4 Hz. Scale bars in A also apply to B and C. *$P < 0.05$.

Action of exogenous DA on STN neurons

Guided by the relatively moderate number of DA-releasing axons in the STN and the relatively moderate levels of DA that were detected, we applied a lower concentration of DA than has been typically utilized in physiological studies addressing the action of DA in the CNS in general (e.g. Gulledge & Stuart, 2003) and the STN in particular (Zhu *et al.*, 2002a,b; Tofighy *et al.*, 2003). Thus in each of six neurons that were recorded in the perforated patch configuration, we observed that 1 μM DA significantly increased the frequency of autonomous activity (Fig. 11A; control mean firing rate = 5.57 ± 2.26 Hz, DA mean firing rate = 6.71 ± 1.88 Hz, $P = 0.031$, WSR test, $n = 6$). In the same neurons an additional effect of 1 μM DA was a reduction in the peak magnitude (Fig. 11B; control GABA-A $IPSP_{mag}$ at −59 mV = −15.33 mV, DA GABA-A $IPSP_{mag}$ at −59 mV = −11.89 mV, $P = 0.031$, WSR test, $n = 6$) and integral (Fig. 11B; control GABA-A $IPSP_{int}$ at −59 mV = −0.972 ± 0.539 mV.s, DA GABA-A $IPSP_{int}$ at

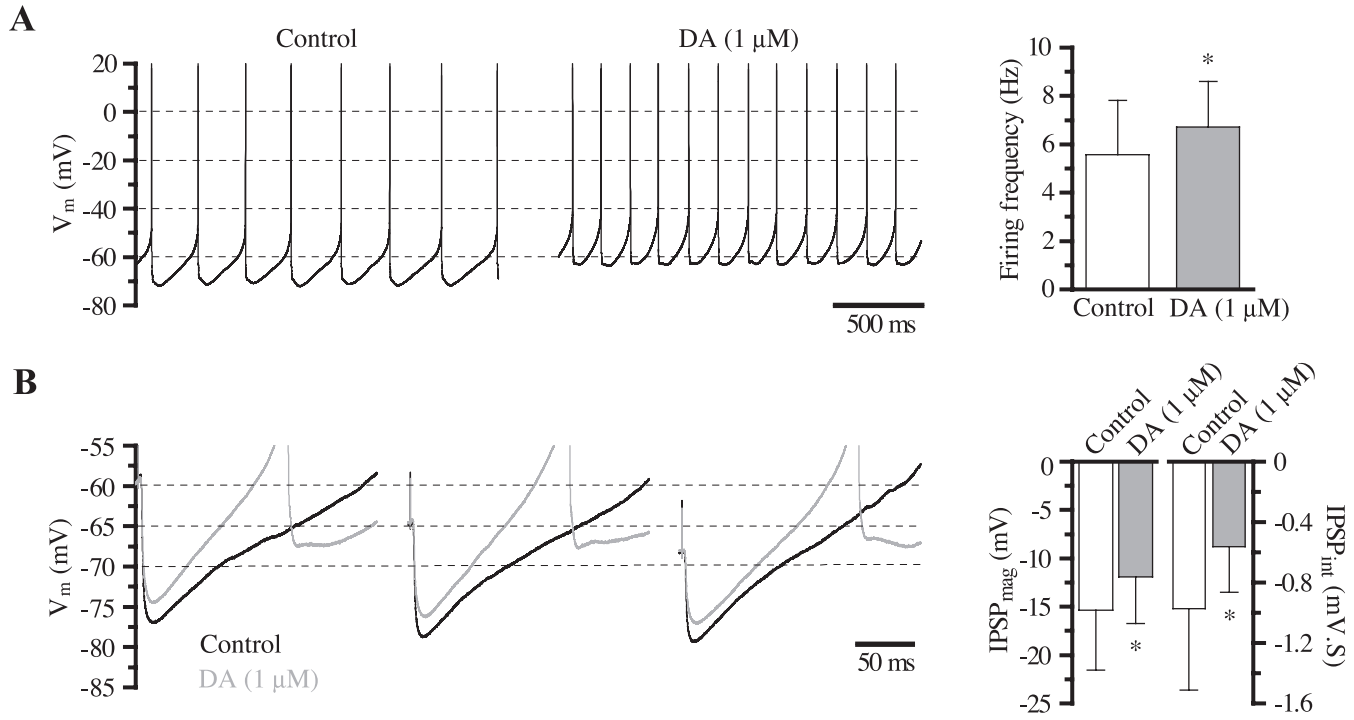

FIG. 11. A low concentration of DA increases the frequency of autonomous oscillation and reduces the impact of inhibitory synaptic transmission in the STN. (A) The effect of 1 μM DA on a typical autonomously active STN neuron. DA increased the frequency of activity and produced a general depolarization. DA at 1 μM produced a similar significant effect (*$P < 0.05$) in the sample population of six neurons. (B) The effect of 1 μM DA on GABA-A IPSPs that were evoked in the same neuron by electrical stimulation of the internal capsule. At membrane potentials associated with autonomous oscillation, the magnitude and integral of GABA-A-IPSPs ($IPSP_{mag}$ and $IPSP_{int}$, respectively) were significantly (*$P < 0.05$) reduced in this neuron and the sample population of six cells. The stimulation artifact (rapid upward transient) denotes the onset of electrical stimulation. Synaptic transmission at AMPA, NMDA and GABA-B receptors was blocked by the continuous application of APV, DNQX and CGP55845 throughout these recordings.

−59 mV = −0.564 ± 0.300 mV.s, $P = 0.031$, WSR test, $n = 6$) of evoked GABA-A IPSPs. These data demonstrate that a low concentration of DA exerts a potent action on the activity of STN neurons and the impact of GABAergic transmission at post-synaptic GABA-A receptors.

Discussion

Synaptic transmission of DA in the STN

In support of previous reports, we found that the STN is innervated by numerous TH-immunoreactive axons (Campbell *et al*., 1985; Lavoie *et al*., 1989; Hassani *et al*., 1997; Cossette *et al*., 1999; Hedreen, 1999; Francois *et al*., 2000). As TH- and DA-immunoreactive axons predominantly formed symmetric synaptic contacts and all DβH-immunoreactive axons formed asymmetric contacts, it is likely that the majority of TH-immunoreactive synapses in the STN are dopaminergic rather than norepinephrinergic. As DA was also observed in axons forming asymmetric synapses, DA may be present in TH-immunoreactive asymmetric synapse-forming axons as a precursor to the synthesis of NE, which is subsequently released and/or as the principal neurotransmitter.

On the basis of FCV, DA rather than NE was the predominant monoamine released following electrical stimulation. The FCV electrodes employed in this study are at least two-fold more sensitive to DA than NE and moreover the peak magnitude and lifetime of the DA-like signal were increased by selective inhibition of the DAT. The release of DA was dependent on extracellular calcium, which is a characteristic of neurotransmitter release via exocytosis (reviewed by Katz, 1996). Finally, DA release was dependent on TTX-sensitive Na_v channels, which implies that action potentials in DA axons were necessary for the evoked release.

Low concentrations of DA are released in the STN

As predicted from the relatively low numbers of DA axons in the STN compared with the striatum, the peak $[DA]_o$ that was detected following electrical stimulation was lower in the STN than in the striatum. Furthermore, multiple stimulus pulses were required to generate detectable $[DA]_o$ in the STN compared with a single stimulus pulse in the striatum. The relative densities of DA release sites are likely to be major factors in determining the concentration and distribution of DA in the extracellular environment (Cragg *et al*., 1997b; Rice *et al*., 1997) but other factors including the regulation of release probability (Cragg & Greenfield, 1997; Cragg, 2003), the tortuosity and volume of extracellular space and the distribution of release sites in relation to the distribution of the DAT are also likely to be influential (Cragg *et al*., 2001; Cragg & Rice, 2004).

Although the $[DA]_o$ detected in the STN was relatively low compared with the striatum, it was similar to the levels detected in the SN (Cragg *et al*., 1997b; Rice *et al*., 1997) where it is known to exert physiological effects (Falkenburger *et al*., 2001). The efficacy of DA depends on whether its target receptors are in their low- or high-affinity states (Richfield *et al*., 1989). Typically, EC50s for DA at D2, D3 (Werner *et al*., 1996; Levant, 1997; Neve & Neve, 1997) and D5 receptors (Weinshank *et al*., 1991; Neve & Neve, 1997; Demchyshyn *et al*., 2000) are in the 2–500 nM range and the EC50s

for D1 receptors are in the high-nM to low-μM range (Neve & Neve, 1997; Demchyshyn *et al*., 2000). Thus, the $[DA]_o$ detected in the STN (as in the SN) would be sufficient to bind to and initiate signal transduction at high-affinity DA receptors. It also likely that lower affinity DA receptors would be activated by the higher $[DA]_o$ that are presumably found adjacent to release sites (Cragg & Rice, 2004).

Low concentrations of DA influence activity and inhibitory synaptic transmission/integration in the STN

Perforated patch clamp recording of STN neurons was employed to maintain the intracellular signalling pathways that may be activated by DA, intrinsic calcium dynamics that are critical to activity, and the natural transmembrane gradient of chloride ions that permeate GABA-A receptors. Under these conditions, 1 μM DA depolarized STN neurons and increased their frequency of autonomous oscillation (~20%), and reduced the magnitude (~22%) and the integral (~44%) of evoked GABA-A IPSPs in STN neurons. These effects are consistent with reports demonstrating: (i) that the activation of post-synaptic D2 receptors leads to the closure of relatively voltage-independent K^+ channels (Zhu *et al*., 2002b), which leads to an increase in the frequency of firing in STN neurons (Zhu *et al*., 2002a,b; Tofighy *et al*., 2003); and (ii) that the activation of presynaptic D2 receptors reduces GABAergic transmission, presumably from the globus pallidus, which leads to a reduction in the magnitude of evoked inhibitory post-synaptic currents (IPSCs; Shen & Johnson, 2000). In general, higher concentrations of DA were applied to STN neurons in those previous studies, or when DA was applied at a similar concentration, the effects were smaller than the effects reported here. These differences may be due to the physiological recording temperature and application of sodium metabisulfite to retard the oxidation of exogenously applied DA in this study. Furthermore, whole cell recordings have previously been shown to attenuate the effects of DA receptor activation in the STN, presumably through the dialysis/perturbation of intracellular molecules involved in signal transduction (Tofighy *et al*., 2003). Our findings demonstrate that DA at a concentration that is similar to that detected by FCV can have a potent action on the degree of hyperpolarization produced by a single GABA-A IPSP. This action presumably arises from the net effect of a reduction in the synaptic release of GABA and post-synaptic depolarization, which increases the activation of intrinsic Na_v channels, which terminate IPSPs more effectively.

Functional implications

The pattern of expression of DA receptor subtypes in STN neurons, examined through *in situ* hybridization, is controversial. Subthalamic neurons have been reported to express D5 receptors (Svenningsson & Le Moine, 2002) or D2–D3 receptors (Hurd *et al*., 2001; supported by Bouthenet *et al*., 1991). Using the RT-PCR technique, Flores *et al*. (1999) have reported the expression of mRNA encoding D1 and D2–D3 receptors in the STN. Physiological studies support the view that STN neurons express both D1-like and D2-like receptors. The activation of D5 receptors increases the contribution of $Ca_v1.2$–1.3 channels to excitability in a subpopulation of STN neurons (Baufreton *et al*., 2003) and the activation of D2 receptors leads to the closure of K^+ channels (Zhu *et al*., 2002b), which increases the frequency of firing in STN neurons (Zhu *et al*., 2002a,b; Tofighy *et al*., 2003; present study). Exogenously applied DA also reduces inhibitory synaptic transmission in the STN (present study) through the activation of presynaptic D2 receptors (Shen & Johnson, 2000). Taken together, these effects could account for the robust excitation of STN neurons, which follows the local application of DA *in vivo* (Campbell *et al*., 1985; Mintz *et al*., 1986; Ni *et al*., 2001).

The increased correlated, rhythmic bursting and mean frequency of STN activity in PD has traditionally not been ascribed to the loss of the direct effects of DA at receptors in the STN (reviewed by Bevan *et al*., 2002b). However, a reduction in post-synaptic D2 receptor activation, which should lead to the hyperpolarization of STN neurons and a reduction in presynaptic D2 receptor activation on GABAergic terminals, which should lead to an increase in GABAergic transmission could, in part, explain the pathological firing pattern if the unusual membrane properties of STN neurons are considered (Nakanishi *et al*., 1987; Beurrier *et al*., 1999; Bevan & Wilson, 1999; Plenz & Kitai, 1999; Otsuka *et al*., 2001; Bevan *et al*., 2002a,b; Hallworth *et al*., 2003). A recent report has shown that as the magnitude of GABA-A IPSPs increase in STN neurons, the more complete the 'phase-reset' of autonomous oscillation and thus the greater the tendency for GABAergic inputs to produce correlated firing (Bevan *et al*., 2002a). Furthermore, STN neurons can respond to bursts of large GABA-A IPSPs with a period of 'post-anodal exaltation' (Andersen & Eccles, 1962) due, in large part, to the de-inactivation of class 3 voltage-dependent Ca^{2+} channels (Beurrier *et al*., 1999; Bevan *et al*., 2000, 2002a; Otsuka *et al*., 2001; Hallworth *et al*., 2003). Post-inhibitory rebound activity can be so intense that the mean level of STN activity is greater in the presence than the absence of GABAergic synaptic transmission (e.g. figs 6 and 8 of Bevan *et al*., 2002a). Furthermore, the tendency for GABA-A IPSPs to generate rebound burst firing is enhanced when the frequency of autonomous activity is reduced (e.g. figs 6 and 8 of Bevan *et al*., 2002a). Thus, the dual action on resting polarization and GABAergic synaptic transmission/integration, which may result from the degeneration of the dopaminergic nigrosubthalamic pathway, could underlie, in part, the abnormal correlated and/or burst activity of STN neurons in PD.

Acknowledgements

This work was supported by NIH-NINDS grants NS04128, NS20702 and NS047085 (M.D.B.), the Medical Research Council (J.P.B.) and a Beit Memorial Fellowship (S.J.C.). We thank Caroline Francis for technical assistance and Joshua Park and Viraj Parikh for assistance with the immunocytochemical experiments.

Abbreviations

ACSF, artificial cerebrospinal fluid; AMPA, α-amino-3-hydroxy-5-methyl-4-isoxazolepropionic-acid; APV, D-(–)-2-amino-5-phosphonopentanoic acid; DA, dopamine; $[DA]_o$, extracellular concentration of dopamine; DAT, dopamine transporter; DβH, dopamine β-hydroxylase; DNQX, 6,7-dinitroquinoxaline-2,3-dione; FCV, fast-scan cyclic voltammetry; GABA, γ-aminobutyric acid; GABAzine, SR 95531 hydrobromide; 5-HT, 5-hydroxytryptamine; IPSP, inhibitory post-synaptic potential; $IPSP_{int}$, inhibitory post-synaptic potential (integral); $IPSP_{mag}$, inhibitory post-synaptic potential (magnitude); M-WU, Mann–Whitney *U*-test; NE, norepinephrine; NMDA, *N*-methyl-D-aspartic acid; PB, phosphate buffer; PBS, phosphate-buffered saline; PD, Parkinson's disease; SN, substantia nigra; STN, subthalamic nucleus; TH, tyrosine hydroxylase; TTX, tetrodotoxin; WSR, Wilcoxon signed-rank test.

References

Abe, Y., Furukawa, K., Itoyama, Y. & Akaike, N. (1994) Glycine response in acutely dissociated ventromedial hypothalamic neuron of the rat: new approach with gramicidin perforated patch-clamp technique. *J. Neurophysiol.*, **72**, 1530–1537.

Andersen, P. & Eccles, J.C. (1962) Inhibitory phasing of neuronal discharge. *Nature*, **196**, 645–647.

Asan, E. (1993) Comparative single and double immunolabelling with antisera against catecholamine biosynthetic enzymes: criteria for the identification of dopaminergic, noradrenergic and adrenergic structures in selected rat brain areas. *Histochemistry*, **99**, 427–442.

Asanuma, C. (1992) Noradrenergic innervation of the thalamic reticular nucleus: a light and electron microscopic immunohistochemical study in rats. *J. Comp. Neurol.*, **319**, 299–311.

Barry, P.H. (1994) JPCalc – a software package for calculating liquid junction potential corrections in patch-clamp, intracellular, epithelial and bilayer measurements and for correcting junction potential measurements. *J. Neurosci. Methods*, **51**, 107–116.

Baufreton, J., Garret, M., Rivera, A., de la Calle, A., Gonon, F., Dufy, B., Bioulac, B. & Taupignon, A. (2003) D5 (not D1) dopamine receptors potentiate burst-firing in neurons of the subthalamic nucleus by modulating an L-type calcium conductance. *J. Neurosci.*, **23**, 816–825.

Benabid, A.L., Koudsie, A., Benazzouz, A., Piallat, B., Krack, P., Limousin-Dowsey, P., Lebas, J.F. & Pollak, P. (2001) Deep brain stimulation for Parkinson's disease. *Adv. Neurol.*, **86**, 405–412.

Beurrier, C., Congar, P., Bioulac, B. & Hammond, C. (1999) Subthalamic nucleus neurons switch from single-spike activity to burst-firing mode. *J. Neurosci.*, **19**, 599–609.

Bevan, M.D., Magill, P.J., Hallworth, N.E., Bolam, J.P. & Wilson, C.J. (2002a) Regulation of the timing and pattern of action potential generation in rat subthalamic neurons *in vitro* by GABA-A IPSPs. *J. Neurophysiol.*, **87**, 1348–1362.

Bevan, M.D., Magill, P.J., Terman, D., Bolam, J.P. & Wilson, C.J. (2002b) Move to the rhythm: oscillations in the subthalamic nucleus–external globus pallidus network. *Trends Neurosci.*, **25**, 525–531.

Bevan, M.D. & Wilson, C.J. (1999) Mechanisms underlying spontaneous oscillation and rhythmic firing in rat subthalamic neurons. *J. Neurosci.*, **19**, 7617–7628.

Bevan, M.D., Wilson, C.J., Bolam, J.P. & Magill, P.J. (2000) Equilibrium potential of GABA (A) current and implications for rebound burst firing in rat subthalamic neurons *in vitro*. *J. Neurophysiol.*, **83**, 3169–3172.

Bolam, J.P. (1992) *Experimental Neuroanatomy: A Practical Approach.* Oxford University Press, Oxford.

Bouthenet, M.L., Souil, E., Martres, M.P., Sokoloff, P., Giros, B. & Schwartz, J.C. (1991) Localization of D3 receptor mRNA in the rat brain using in situ hybridization histochemistry: comparison with dopamine D2 receptor mRNA. *Brain Res.*, **564**, 203–219.

Brown, L.L., Markman, M.H., Wolfson, L.I., Dvorkin, B., Warner, C. & Katzman, R. (1979) A direct role of dopamine in the rat subthalamic nucleus and an adjacent intrapeduncular area. *Science*, **206**, 1416–1418.

Campbell, G.A., Eckardt, M.J. & Weight, F.F. (1985) Dopaminergic mechanisms in subthalamic nucleus of rat: analysis using horseradish peroxidase and microiontophoresis. *Brain Res.*, **333**, 261–270.

Chagnaud, J.L., Mons, N., Tuffet, S., Grandier-Vazeilles, X. & Geffard, M. (1987) Monoclonal antibodies against glutaraldehyde-conjugated dopamine. *J. Neurochem.*, **49**, 487–494.

Chang, H.T. (1989) Noradrenergic innervation of the substantia innominata: a light and electron microscopic analysis of dopamine beta-hydroxylase immunoreactive elements in the rat. *Exp. Neurol.*, **104**, 101–112.

Cossette, M., Levesque, M. & Parent, A. (1999) Extrastriatal dopaminergic innervation of human basal ganglia. *Neurosci. Res.*, **34**, 51–54.

Cragg, S.J. (2003) Variable dopamine release probability and short-term plasticity between functional domains of the primate striatum. *J. Neurosci.*, **23**, 4378–4385.

Cragg, S.J. & Greenfield, S.A. (1997) Differential autoreceptor control of somatodendritic and axon terminal dopamine release in substantia nigra, ventral tegmental area and striatum. *J. Neurosci.*, **17**, 5738–5746.

Cragg, S.J., Hawkey, C.R. & Greenfield, S.A. (1997a) Comparison of serotonin and dopamine release in substantia nigra and ventral tegmental area: region and species differences. *J. Neurochem.*, **69**, 2378–2386.

Cragg, S.J., Holmes, C., Hawkey, C.R. & Greenfield, S.A. (1998) Dopamine is released spontaneously from developing midbrain neurons in organotypic culture. *Neuroscience*, **84**, 325–330.

Cragg, S.J., Nicholson, C., Kume-Kick, J., Tao, L. & Rice, M.E. (2001) Dopamine-mediated volume transmission in midbrain is regulated by distinct extracellular geometry and uptake. *J. Neurophysiol.*, **85**, 1761–1771.

Cragg, S.J. & Rice, M.E. (2004) DAncing past the DAT at a DA synapse. *Trends Neurosci.*, **27**, 270–277.

Cragg, S.J., Rice, M.E. & Greenfield, S.A. (1997b) Heterogeneity of electrically evoked dopamine release and reuptake in substantia nigra, ventral tegmental area, and striatum. *J. Neurophysiol.*, **77**, 863–873.

DeLong, M.R. (1990) Primate models of movement disorders of basal ganglia origin. *Trends Neurosci.*, **13**, 281–285.

Demchyshyn, L.L., McConkey, F. & Niznik, H.B. (2000) Dopamine D5 receptor agonist high affinity and constitutive activity profile conferred by carboxyl-terminal tail sequence. *J. Biol. Chem.*, **275**, 23446–23455.

Descarries, L., Watkins, K.C., Garcia, S., Bosler, O. & Doucet, G. (1996) Dual character, asynaptic and synaptic, of the dopamine innervation in adult rat neostriatum: a quantitative autoradiographic and immunocytochemical analysis. *J. Comp. Neurol.*, **375**, 167–186.

Dodt, H.U., D'Arcangelo, G. & Zieglgansberger, W. (1999) Infrared videomicroscopy. In Yuste, R., Lanni, F. & Konnerth, A. (Eds), *Imaging Neurons. A Laboratory Manual.* Cold Spring Harbor Laboratory Press, New York, pp. 7.1–7.8.

Falkenburger, B.H., Barstow, K.L. & Mintz, I.M. (2001) Dendrodendritic inhibition through reversal of dopamine transport. *Science*, **293**, 2465–2470.

Flores, G., Liang, J.J., Sierra, A., Martinez-Fong, D., Quirion, R., Aceves, J. & Srivastava, L.K. (1999) Expression of dopamine receptors in the subthalamic nucleus of the rat: characterization using reverse transcriptase-polymerase chain reaction and autoradiography. *Neuroscience*, **91**, 549–556.

Francois, C., Savy, C., Jan, C., Tande, D., Hirsch, E.C. & Yelnik, J. (2000) Dopaminergic innervation of the subthalamic nucleus in the normal state, in MPTP-treated monkeys, and in Parkinson's disease patients. *J. Comp. Neurol.*, **425**, 121–129.

Gulledge, A.T. & Stuart, G.J. (2003) Action potential initiation and propagation in layer 5 pyramidal neurons of the rat prefrontal cortex: absence of dopamine modulation. *J. Neurosci.*, **23**, 11363–11372.

Hallworth, N.E., Wilson, C.J. & Bevan, M.D. (2003) Apamin-sensitive small conductance calcium-activated potassium channels, through their selective coupling to voltage-gated calcium channels, are critical determinants of the precision, pace, and pattern of action potential generation in rat subthalamic nucleus neurons *in vitro*. *J. Neurosci.*, **23**, 7525–7542.

Hassani, O.K., Francois, C., Yelnik, J. & Feger, J. (1997) Evidence for a dopaminergic innervation of the subthalamic nucleus in the rat. *Brain Res.*, **749**, 88–94.

Hedreen, J.C. (1999) Tyrosine hydroxylase-immunoreactive elements in the human globus pallidus and subthalamic nucleus. *J. Comp. Neurol.*, **409**, 400–410.

Hurd, Y.L., Suzuki, M. & Sedvall, G.C. (2001) D1 and D2 dopamine receptor mRNA expression in whole hemisphere sections of the human brain. *J. Chem. Neuroanat.*, **22**, 127–137.

Jones, S.R., Garris, P.A., Kilts, C.D. & Wightman, R.M. (1995) Comparison of dopamine uptake in the basolateral amygdaloid nucleus, caudate-putamen, and nucleus accumbens of the rat. *J. Neurochem.*, **64**, 2581–2589.

Karle, E.J., Anderson, K.D., Medina, L. & Reiner, A. (1996) Light and electron microscopic immunohistochemical study of dopaminergic terminals in the striatal portion of the pigeon basal ganglia using antisera against tyrosine hydroxylase and dopamine. *J. Comp. Neurol.*, **369**, 109–124.

Katz, B. (1996) Neural transmitter release: from quantal secretion to exocytosis and beyond. The Fenn Lecture. *J. Neurocytol.*, **25**, 677–686.

Kyrozis, A. & Reichling, D.B. (1995) Perforated-patch recording with gramicidin avoids artifactual changes in intracellular chloride concentration. *J. Neurosci. Methods*, **57**, 27–35.

Lavoie, B., Smith, Y. & Parent, A. (1989) Dopaminergic innervation of the basal ganglia in the squirrel monkey as revealed by tyrosine hydroxylase immunohistochemistry. *J. Comp. Neurol.*, **289**, 36–52.

Levant, B. (1997) The D3 dopamine receptor: neurobiology and potential clinical relevance. *Pharmacol. Rev.*, **49**, 231–252.

Levi, G. & Raiteri, M. (1993) Carrier-mediated release of neurotransmitters. *Trends Neurosci.*, **16**, 415–419.

Meibach, R.C. & Katzman, R. (1979) Catecholaminergic innervation of the subthalamic nucleus: evidence for a rostral continuation of the A9 (substantia nigra) dopaminergic cell group. *Brain Res.*, **173**, 364–368.

Mintz, I., Hammond, C. & Feger, J. (1986) Excitatory effect of iontophoretically applied dopamine on identified neurons of the rat subthalamic nucleus. *Brain Res.*, **375**, 172–175.

Myers, V.B. & Haydon, D.A. (1972) Ion transfer across lipid membranes in the presence of gramicidin A. II. The ion selectivity. *Biochim. Biophys. Acta*, **274**, 313–322.

Nakanishi, H., Kita, H. & Kitai, S.T. (1987) Electrical membrane properties of rat subthalamic neurons in an *in vitro* slice preparation. *Brain Res.*, **437**, 35–44.

Neher, E. (1992) Corrections for liquid junction potentials in patch-clamp experiments. *Methods Enzymol.*, **207**, 123–131.
Neve, K.A. & Neve, R.L. (1997) Molecular biology of dopamine receptors. In Neve, K.A. & Neve, R.L. (Eds), *The Dopamine Receptors*. Humana, Totowa, NJ, pp. 27–76.
Ni, Z., Gao, D., Bouali-Benazzouz, R., Benabid, A.L. & Benazzouz, A. (2001) Effect of microiontophoretic application of dopamine on subthalamic nucleus neuronal activity in normal rats and in rats with unilateral lesion of the nigrostriatal pathway. *Eur. J. Neurosci.*, **14**, 373–381.
Otsuka, T., Murakami, F. & Song, W.J. (2001) Excitatory postsynaptic potentials trigger a plateau potential in rat subthalamic neurons at hyperpolarized states. *J. Neurophysiol.*, **86**, 1816–1825.
Parry, T.J., Eberle-Wang, K., Lucki, I. & Chesselet, M.F. (1994) Dopaminergic stimulation of subthalamic nucleus elicits oral dyskinesia in rats. *Exp. Neurol.*, **128**, 181–190.
Plenz, D. & Kitai, S.T. (1999) A basal ganglia pacemaker formed by the subthalamic nucleus and external globus pallidus. *Nature*, **400**, 677–682.
Rice, M.E., Cragg, S.J. & Greenfield, S.A. (1997) Characteristics of electrically evoked somatodendritic dopamine release in substantia nigra and ventral tegmental area *in vitro*. *J. Neurophysiol.*, **77**, 853–862.
Richfield, E.K., Penney, J.B. & Young, A.B. (1989) Anatomical and affinity state comparisons between dopamine D1 and D2 receptors in the rat central nervous system. *Neuroscience*, **30**, 767–777.
Schmitz, Y., Benoit-Marand, M., Gonon, F. & Sulzer, D. (2003) Presynaptic regulation of dopaminergic neurotransmission. *J. Neurochem.*, **87**, 273–289.
Seguela, P., Watkins, K.C. & Descarries, L. (1988) Ultrastructural features of dopamine axon terminals in the anteromedial and the suprarhinal cortex of adult rat. *Brain Res.*, **442**, 11–22.
Seguela, P., Watkins, K.C., Geffard, M. & Descarries, L. (1990) Noradrenaline axon terminals in adult rat neocortex: an immunocytochemical analysis in serial thin sections. *Neuroscience*, **35**, 249–264.
Sesack, S.R. (2002) Synaptology of dopamine neurons. In Di Chiara, G. (Ed.), *Dopamine in the CNS I*. Springer-Verlag, Berlin, pp. 63–119.
Shen, K.Z. & Johnson, S.W. (2000) Presynaptic dopamine D2 and muscarine M3 receptors inhibit excitatory and inhibitory transmission to rat subthalamic neurones *in vitro*. *J. Physiol. (Lond.)*, **525**, 331–341.
Shen, K.Z., Zhu, Z.T., Munhall, A. & Johnson, S.W. (2003) Dopamine receptor supersensitivity in rat subthalamus after 6-hydroxydopamine lesions. *Eur. J. Neurosci.*, **18**, 2967–2974.
Smith, A.D. & Bolam, J.P. (1990) The neural network of the basal ganglia as revealed by the study of synaptic connections of identified neurones. *Trends Neurosci.*, **13**, 259–265.
Smith, Y. & Kieval, J.Z. (2000) Anatomy of the dopamine system in the basal ganglia. *Trends Neurosci.*, **23**, S228–S233.
Sulzer, D., Chen, T.K., Lau, Y.Y., Kristensen, H., Rayport, S. & Ewing, A. (1995) Amphetamine redistributes dopamine from synaptic vesicles to the cytosol and promotes reverse transport. *J. Neurosci.*, **15**, 4102–4108.
Svenningsson, P. & Le Moine, C. (2002) Dopamine D1/5 receptor stimulation induces c-fos expression in the subthalamic nucleus: possible involvement of local D5 receptors. *Eur. J. Neurosci.*, **15**, 133–142.
Tofighy, A., Abbott, A., Centonze, D., Cooper, A.J., Noor, E., Pearce, S.M., Puntis, M., Stanford, I.M., Wigmore, M.A. & Lacey, M.G. (2003) Excitation by dopamine of rat subthalamic nucleus neurones *in vitro* – a direct action with unconventional pharmacology. *Neuroscience*, **116**, 157–166.
Voorn, P., Jorritsma-Byham, B., Van Dijk, C. & Buijs, R.M. (1986) The dopaminergic innervation of the ventral striatum in the rat: a light- and electron-microscopical study with antibodies against dopamine. *J. Comp. Neurol.*, **251**, 84–99.
Weinshank, R.L., Adham, N., Macchi, M., Olsen, M.A., Branchek, T.A. & Hartig, P.R. (1991) Molecular cloning and characterization of a high affinity dopamine receptor (D1 beta) and its pseudogene. *J. Biol. Chem.*, **266**, 22427–22435.
Werner, P., Hussy, N., Buell, G., Jones, K.A. & North, R.A. (1996) D2, D3, and D4 dopamine receptors couple to G protein-regulated potassium channels in *Xenopus* oocytes. *Mol. Pharmacol.*, **49**, 656–661.
Wise, S.P., Murray, E.A. & Gerfen, C.R. (1996) The frontal cortex–basal ganglia system in primates. *Crit. Rev. Neurobiol.*, **10**, 317–356.
Zhu, Z., Bartol, M., Shen, K. & Johnson, S.W. (2002a) Excitatory effects of dopamine on subthalamic nucleus neurons: *in vitro* study of rats pretreated with 6-hydroxydopamine and levodopa. *Brain Res.*, **945**, 31–40.
Zhu, Z.T., Shen, K.Z. & Johnson, S.W. (2002b) Pharmacological identification of inward current evoked by dopamine in rat subthalamic neurons *in vitro*. *Neuropharmacology*, **42**, 772–781.